Free-electron lasers

Peter Schmüser
Institut für Experimentalphysik, Universität Hamburg, Germany

Abstract
The synchrotron radiation of relativistic electrons in undulator magnets and the low-gain Free-Electron Laser (FEL) are discussed in some detail. The high-gain FEL based on the principle of Self Amplified Spontaneous Emission is treated on a qualitative level.

1 Introduction

The Free-Electron Laser (FEL) principle has been known since the early 1970's but for many years FEL's have played a marginal role in comparison with conventional lasers. Only in recent years it has become clear that these devices have the potential of becoming exceedingly powerful light sources in the vacuum-ultraviolet (VUV) and X ray regime. In my talk I will first deal with undulator radiation since it is intimitely related to FEL radiation, then explain the low-gain FEL and finally treat the high-gain FEL based on the principle of Self Amplified Spontaneous Emission (SASE). SASE-FEL's are frequently considered as the fourth generation of accelerator-based light sources. In contrast to existing synchrotron radiation light sources which are mostly storage rings the FEL requirements on the electron beam quality in terms of low transverse emittance and small energy spread are so demanding that only linear accelerators can be used to provide the drive beam.

In my one-hour talk it was not possible to go much into mathematical details. The high-gain FEL is therefore treated only qualitatively. For a thorough presentation of SASE FEL's I refer to the book "The Physics of Free Electron Lasers" by Saldin, Schneidmiller and Yurkov and to the lectures by J. Rossbach at the CERN Accelerator School on Synchrotron Radiation.

1.1 Electron accelerators as light sources

In the bending magnets of a high-energy circular accelerator the relativistic electrons emit synchrotron radiation. For a Lorentz factor[1] $\gamma = W/(m_e c^2) \gg 1$ the radiation is emitted almost tangentially to the circular orbit. The frequency spectrum is continuous and extends from zero to frequencies beyond the "critical frequency"

$$\omega_c = \frac{3c\gamma^3}{2R} \tag{1}$$

where R is the radius of curvature in the bending magnet. The radiation power is

$$P_{\text{rad}} = \frac{e^2 c}{6\pi\varepsilon_0}\,\frac{\gamma^4}{R^2}\ . \tag{2}$$

In modern synchrotron light sources the radiation used for research is produced in wiggler or undulator magnets which are periodic arrangements of many short dipole magnets of alternating polarity. The electrons move on a wavelike orbit through such a magnet (Fig. 1) but the overall deflection of the beam is zero. Undulator radiation is far more useful than bending-magnet radiation because it is nearly monochromatic and concentrated in a narrow angular cone with an opening angle of about $\pm 1/\gamma$. The wavelength can be estimated from the following consideration. Call λ_u the period of the magnet arrangement. In a coordinate system moving with the average speed of the beam, the relativistic length contraction reduces the period to $\lambda_u^* = \lambda_u/\gamma$, and the electrons oscillate at a correspondingly higher

[1] The total relativistic energy of the electron is denoted by W since in this article the letter E is reserved for electric fields.

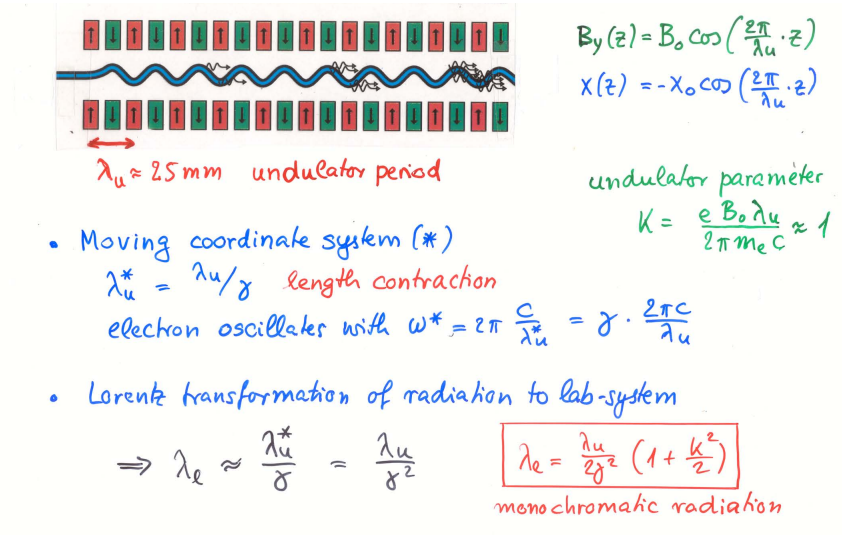

Fig. 1: Schematic representation of undulator radiation. For simplicity the alternating magnetic field and the cosine-like electron orbit have been drawn in the same plane.

frequency $\omega^* = 2\pi c/\lambda_u^* = \gamma\, 2\pi c/\lambda_u$ and emit dipole radiation. If one Lorentz-transforms this radiation into the laboratory system one gets for the light wavelength $\lambda_\ell \approx \lambda_u^*/\gamma = \lambda_u/\gamma^2$; for example, for a Lorentz factor $\gamma = 1000$ (an electron energy of 511 MeV) the radiation wavelength is a million times shorter than the undulator period. Moreover, the wavelength can be easily varied by changing the particle energy.

It is interesting to note that the total energy radiated by a relativistic electron in an undulator is the same as that in a bending magnet of equal magnetic length, however, the intensity is concentrated in a narrow spectral range. Different electrons radiate independently in bending magnets as well as in undulators, hence the total power produced by a bunch of N electrons is simply N times the radiation power of one electron.

1.2 Free-electron and conventional lasers

The next big improvement is given by the Free-Electron Laser. The main component is again an undulator magnet but by means of a clever mechanism (explained below) one forces a large number of electrons to emit their radiation coherently. Like undulator radiation, the FEL radiation is almost monochromatic and well collimated but the power will be N times higher if one manages to achieve full coherence in the bunch.

A conventional laser (Fig. 2) consists of three basic components: the laser medium with at least 3 energy levels, an energy pump which creates a population inversion, and an optical resonator. The electrons are bound to atomic, molecular or solid-state levels, so one may call this a "bound-electron" laser in contrast to the free-electron laser where the electrons move in vacuum. In an FEL (Fig. 3) the role of the active laser medium and the energy pump are both taken over by the relativistic electron beam. An optical cavity is no longer possible for wavelengths below 100 nm, because the reflectivity of metals and other mirror coatings drops quickly to zero at normal incidence. Here one has to rely on the principle of Self Amplified Spontaneous Emission (SASE) where the laser gain is achieved in a single passage of a very long undulator magnet. The schematic setup of a SASE FEL is shown in Fig. 4. One big advantage of an FEL in comparison with a conventional laser is the free tunability of the wavelength by simply changing the electron energy.

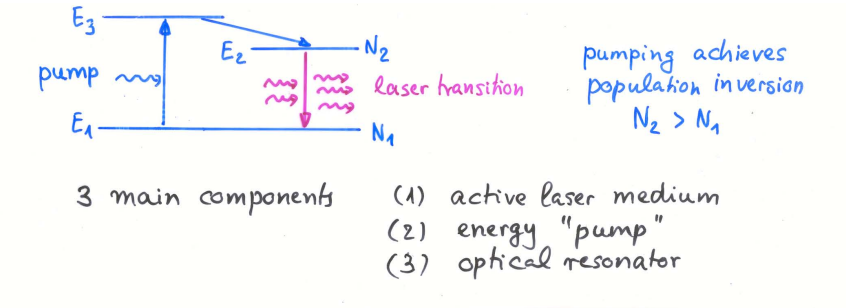

Fig. 2: Scheme of a conventional laser ("bound-electron" laser).

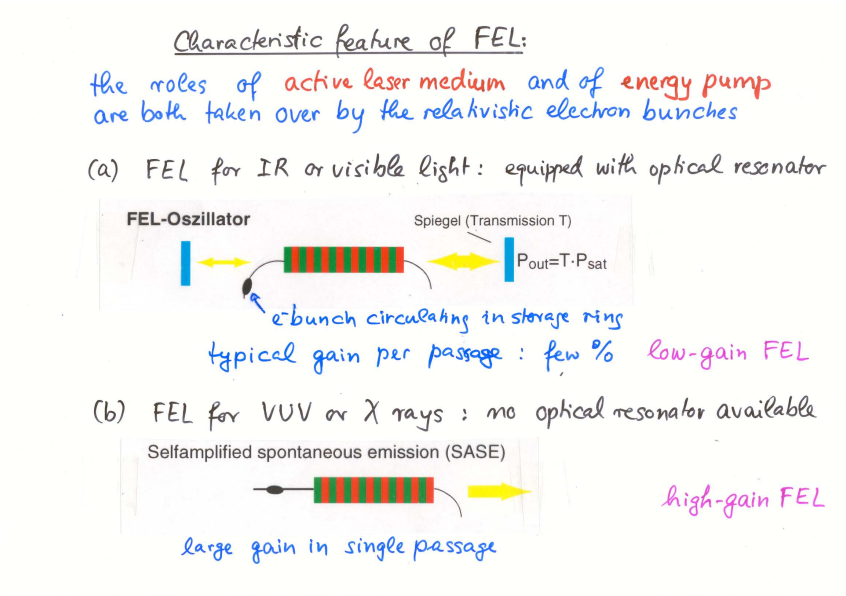

Fig. 3: Principle of free-electron laser. For visible or infrared light an optical resonator can be used. In the ultraviolet and X ray region one has to rely on the mechanism of Self Amplified Spontaneous Emission where the laser gain is achieved in a single passage of a very long undulator.

2 Undulator radiation

2.1 Magnetic field of undulator

The motion of an electron in an undulator magnet is shown schematically in Fig. 5. The undulator axis is along the direction of the beam (z direction), the magnetic field points in the y direction (vertical). The period of the magnet arrangement λ_u is in the order of 25 mm. For simplicity we assume that the horizontal width of the pole shoes is larger than λ_u, then the x dependence of the field can be neglected. The field on the axis is approximately harmonic

$$B_y(0,0,z) = B_0 \cos(k_u z) \quad \text{with} \quad k_u = 2\pi/\lambda_u \tag{3}$$

In vacuum we have $\vec{\nabla} \times \vec{B} = 0$, hence the magnetic field can be written as the gradient of a scalar magnetic potential

$$\vec{B} = \nabla\phi \; .$$

The potential ϕ fulfills the Laplace equation

$$\nabla^2\phi = 0 \; .$$

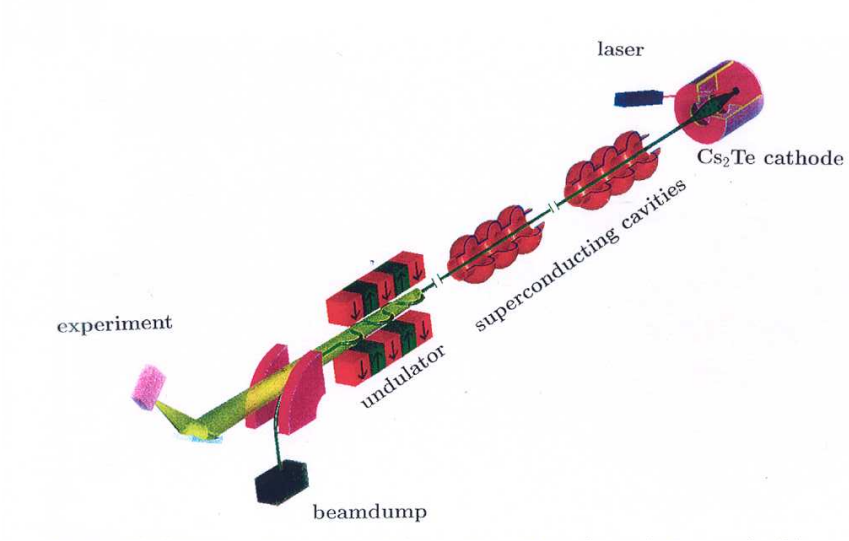

Fig. 4: Schematic of the SASE FEL at the TESLA Test Facility.

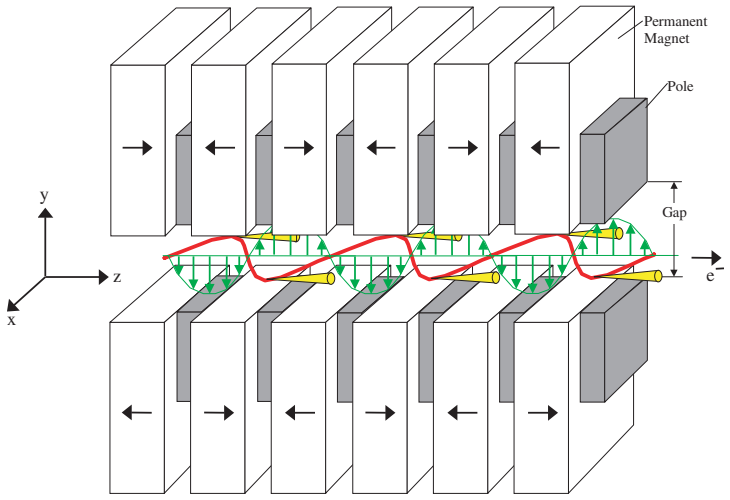

Fig. 5: Schematic view of an undulator magnet with alternating polarity of the magnetic field and of the cosine-like trajectory of the electrons. The distance between two equal poles is called the undulator period λ_u.

Making the ansatz

$$\phi(y,z) = f(y)\cos(k_u z) \quad \Rightarrow \quad \frac{d^2 f}{dy^2} - k_u^2 f = 0$$

we get for the general solution

$$f(y) = c_1 \sinh(k_u y) + c_2 \cosh(k_u y) \ ,$$

$$B_y(y,z) = \frac{\partial \phi}{\partial y} = k_u (c_1 \cosh(k_u y) + c_2 \sinh(k_u y)) \cos(k_u z) \ .$$

The vertical field component B_y is symmetric with respect to the plane $y = 0$ hence $c_2 = 0$, and moreover $k_u c_1 = B_0$. So the potential is

$$\phi(x,y,z) = \frac{B_0}{k_u} \sinh(k_u y) \cos(k_u z) \ . \tag{4}$$

For $y \neq 0$ the magnetic field has also a longitudinal component B_z.

$$\begin{aligned} B_x &= 0 \\ B_y &= B_0 \cosh(k_u y) \cos(k_u z) \\ B_z &= -B_0 \sinh(k_u y) \sin(k_u z) \ . \end{aligned} \tag{5}$$

In the following we restrict ourselves to the symmetry plane $y = 0$.

2.2 Electron Motion in an Undulator

2.2.1 Trajectory in first order

We call $W = E_{kin} + m_e c^2 = \gamma m_e c^2$ the total relativistic energy of the electron. The transverse acceleration by the Lorentz force is

$$\gamma m_e \dot{\vec{v}} = -e\vec{v} \times \vec{B} \ . \tag{6}$$

This results in two coupled equations

$$\ddot{x} = \frac{e}{\gamma m_e} B_y \dot{z} \qquad\qquad \ddot{z} = -\frac{e}{\gamma m_e} B_y \dot{x} \tag{7}$$

which are solved iteratively. To obtain the first-order solution we observe that $v_z = \dot{z} \approx v = \beta\, c = const$ and $v_x \ll v_z$. Then $\ddot{z} \approx 0$ and

$$x(t) \approx -\frac{eB_0}{\gamma m_e \beta c k_u^2} \cos(k_u \beta c t) \ , \qquad z(t) \approx \beta c t \ . \tag{8}$$

The electron travels on a cosine-like trajectory

$$x(z) = -A \cos(k_u z) \quad \text{with} \quad A = \frac{eB_0}{\gamma m_e \beta c k_u^2} \ .$$

The maximum divergence angle is

$$\theta_{max} \approx \left[\frac{dx}{dz}\right]_{max} = \frac{eB_0}{\gamma m_e \beta c k_u} = \frac{K}{\beta\gamma}$$

Here we have introduced the *undulator parameter*

$$K = \frac{eB_0}{m_e c k_u} = \frac{eB_0 \lambda_u}{2\pi m_e c} \ . \tag{9}$$

Synchrotron radiation of relativistic electrons is emitted inside a cone with opening angle $1/\gamma$. If the particle trajectory stays within this cone one speaks of an undulator magnet (Fig. 6):
Undulator: $\theta_{max} \leq 1/\gamma \quad \Rightarrow \quad K \leq 1$.
If the trajectory extends beyond the cone the magnet is called a wiggler:
Wiggler: $K > 1$.
The special feature of an undulator is that the radiated field of an electron interferes with itself along the magnet axis. The consequence is, as we shall see, that the radiation is nearly monochromatic.

2.2.2 Motion in second order

Due to the cosine-trajectory the z component of the velocity is not constant. It is given by

$$v_z = \sqrt{v^2 - v_x^2} \approx c\left(1 - \frac{1}{2\gamma^2}\left(1 + \gamma^2 v_x^2/c^2\right)\right) \ .$$

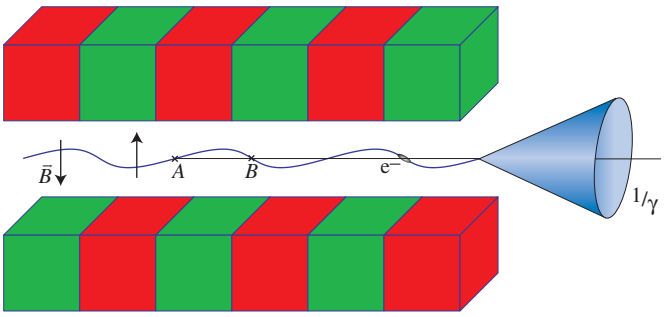

Fig. 6: Schematic view of undulator radiation .

We insert for $v_x = \dot{x}(t)$ the first-order solution, then the average z velocity is

$$\bar{v}_z = c\left(1 - \frac{1}{2\gamma^2}\,(1 + K^2/2)\right) \equiv \bar{\beta}c \tag{10}$$

It should be noted that the z velocity oscillates about the average[2]

$$\dot{z}(t) = \bar{\beta}c + \frac{cK^2}{4\gamma^2}\cos(2\omega_u t) \quad \text{with} \quad \omega_u = \bar{\beta}ck_u \ .$$

The trajectory in second order reads

$$x(t) = -\frac{cK}{\gamma\omega_u}\cos(\omega_u t)\ , \qquad z(t) = \bar{\beta}ct + \frac{cK^2}{8\gamma^2\omega_u}\sin(2\omega_u t)\ . \tag{11}$$

2.2.3 Lorentz transformation into a moving coordinate system

Consider a coordinate system (x^*, y^*, z^*) moving with the average z velocity of the electrons:

$$\bar{v}_z = \bar{\beta}c, \quad \bar{\gamma} \approx \gamma = W/(m_e c^2)\ .$$

The Lorentz transformation reads

$$\begin{aligned} t^* &= \bar{\gamma}(t - \bar{\beta}z/c) = \bar{\gamma}t(1 - \bar{\beta}^2) \approx t/\gamma \\ x^* &= x = -\frac{cK}{\gamma\omega_u}\cos(\omega_u t) \\ z^* &= \bar{\gamma}(z - \bar{\beta}ct) \approx \frac{cK^2}{8\gamma\omega_u}\sin(2\omega_u t) \end{aligned}$$

The electron orbit in the moving system is:

$$x^*(t^*) = -\frac{cK}{\gamma\omega_u}\cos(\omega^* t^*)\ , \qquad z^*(t^*) = \frac{cK^2}{8\gamma\omega_u}\sin(2\omega^* t^*) \tag{12}$$

with $\omega^* = \gamma\omega_u$. Note that $\omega_u t = \omega^* t^*$. This is mainly a transverse harmonic oscillation with the frequency $\omega^* = \gamma\omega_u$. Superimposed is a small longitudinal oscillation which will be ignored here, it leads to higher harmonics in the radiation. The motion is plotted in Fig. 7. In the moving system the electron emits dipole radiation with the frequency $\omega^* = \gamma\omega_u$ and the wavelength $\lambda_u^* = \lambda_u/\gamma$.

[2] This oscillation leads to odd higher harmonics of the undulator radiation, see for example the book by K. Wille. In a helical undulator the z velocity is constant.

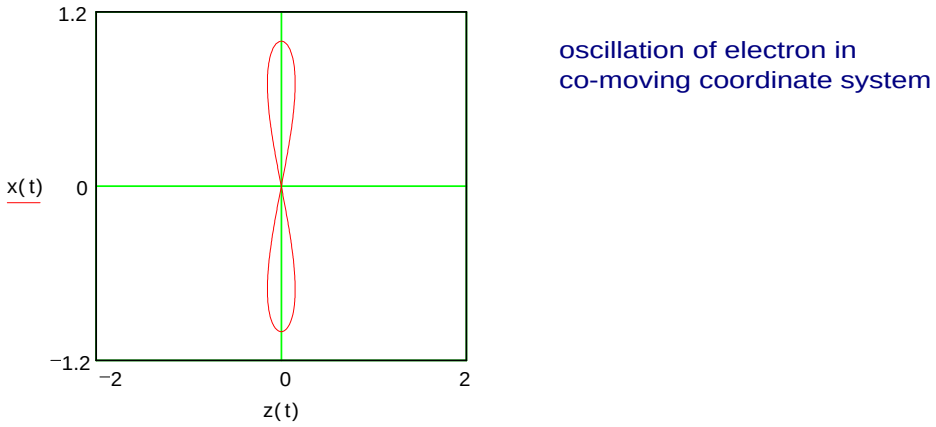

Fig. 7: Oscillation of the electron in the moving coordinate system.

Fig. 8: Radiation characteristics in the laboratory system of an oscillating dipole moving at speeds close to c.

2.2.4 Transformation of radiation into laboratory system

The radiation characteristics of an oscillating dipole moving at relativistic speed is depicted in Fig. 8. Within increasing Lorentz factor γ the radiation becomes more and more concentrated in the forward direction. We are interested in the light wavelength in the laboratory system as a function of the angle θ with respect to the beam axis. The Lorentz transformation of the photon energy reads

$$\hbar\omega^* = \bar{\gamma}\hbar\omega_\ell(1 - \bar{\beta}\cos\theta)$$

$$\Rightarrow \quad \lambda_\ell = \frac{2\pi c}{\omega_\ell} = \frac{2\pi c\bar{\gamma}}{\omega^*}(1 - \bar{\beta}\cos\theta) = \lambda_u(1 - \bar{\beta}\cos\theta)$$

Using $\bar{\gamma} \approx \gamma$, $\bar{\beta} = \left(1 - \frac{1}{2\gamma^2}\left(1 + K^2/2\right)\right)$ and $\cos\theta \approx 1 - \theta^2/2$ we obtain for the wavelength of undulator radiation

$$\lambda_\ell = \frac{\lambda_u}{2\gamma^2}\left(1 + K^2/2 + \gamma^2\theta^2\right) . \tag{13}$$

2.3 Line shape of undulator radiation

An electron passing an undulator with N_u periods produces a wavetrain with N_u oscillations (Fig. 9). The electric field of the light wave is written as

$$E_\ell(t) = \begin{cases} E_0 e^{i\omega_\ell t} & \text{if } -T/2 < t < T/2 \\ 0 & \text{otherwise} \end{cases}$$

The time duration of the wave train is $T = N_u\lambda_\ell/c$. Due to its finite length, this wave train is not

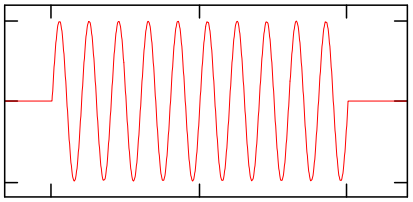

Fig. 9: A finite wavetrain.

monochromatic but contains a frequency spectrum which is obtained by Fourier transformation

$$\begin{aligned} A(\omega) &= \frac{1}{\sqrt{2\pi}} \int_{-\infty}^{+\infty} E_\ell(t) e^{-i\omega t} dt = \frac{E_0}{\sqrt{2\pi}} \int_{-T/2}^{+T/2} e^{i(\omega_\ell - \omega)t} dt \\ &= \frac{2E_0}{\sqrt{2\pi}} \cdot \frac{\sin(\Delta\omega T/2)}{\Delta\omega} \quad \text{with} \quad \Delta\omega = \omega - \omega_\ell \ . \end{aligned}$$

The spectral intensity is

$$I(\omega) \propto \left(\frac{\sin \xi}{\xi} \right)^2 \quad \text{with} \quad \xi = \Delta\omega T/2 = \frac{\pi \, N_u(\omega - \omega_\ell)}{\omega_\ell} \ .$$

It has a maximum at $\omega = \omega_\ell$ and a width proportional to $1/N_u$. The line shape for a wave train with 100 oscillations is shown in Fig. 10. The spectral resolution is

$$\Delta\lambda/\lambda = 1/N_u$$

and amounts to 1% in the present example.

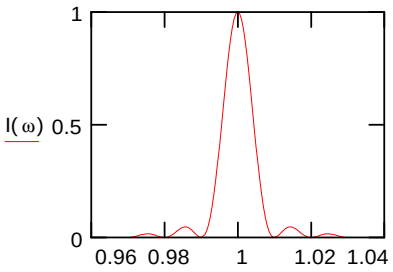

Spectral intensity for a wave train
with N_u = 100 periods

Fig. 10: Normalized spectral intensity distribution of undulator radiation in a magnet with $N_u = 100$ periods.

3 Low-gain FEL

3.1 Energy transfer from electron beam to light wave

We consider the case of "seeding", where the initial light wave with wavelength λ_ℓ is provided by an external source such as an optical laser. The schematic setup of a low-gain FEL is shown in Fig. 11.

The light wave is co-propagating with the relativistic electron beam and is described by a plane electromagnetic wave

$$E_x(z,t) = E_0 \cos(k_\ell z - \omega_\ell t + \psi_0) \quad \text{with} \quad k_\ell = \omega_\ell / c = 2\pi/\lambda_\ell \ .$$

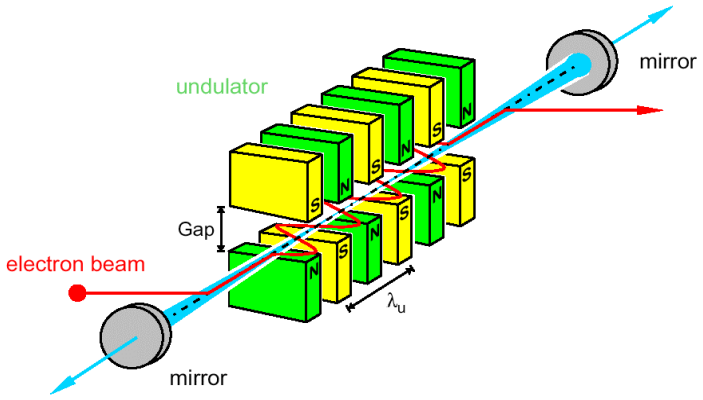

Fig. 11: Principle of low-gain FEL with optical resonator.

Obviously the light wave, travelling with speed c along the z axis, slips with respect to the electrons whose average speed in z direction is

$$\bar{v}_z = c\left(1 - \frac{1}{2\gamma^2}\left(1 + K^2/2\right)\right) \; < \; c \; .$$

The question is then: how can there be a continuous energy transfer from the electron beam to the light wave? The electron energy $W = \gamma m_e c^2$ changes in the time interval dt by

$$dW = \vec{v} \cdot \vec{F} dt = -e v_x(t) E_x(t) dt \; .$$

The x component of the electron velocity v_x and the electric vector E_x of the light wave must point in the same direction to get an energy transfer from the electron to the light wave. To determine the condition for energy transfer along the entire trajectory we compute the electron and light travel times for a half period of the undulator:

$$t_{el} = \lambda_u/(2\bar{v}_z), \quad t_{light} = \lambda_u/(2c) \; .$$

Figure 12 illustrates that after a half period v_x and E_x are still parallel if the phase of the light wave has slipped by π, i.e.

$$\omega_\ell (t_{el} - t_{light}) = \pi \; .$$

(Remark: also $3\pi, 5\pi \ldots$ are possible, leading to higher harmonics of the radiation). This condition allows to compute the light wavelength:

$$\lambda_\ell = \frac{\lambda_u}{2\gamma^2}\left(1 + \frac{K^2}{2}\right)$$

which is identical with the wavelength of undulator radition (in forward direction).

3.1.1 Quantitative treatment

The energy transfer from an electron to the light wave is

$$\begin{aligned} \frac{dW}{dt} &= -e v_x(t) E_x(t) \\ &= -e\frac{cK}{\gamma} \sin(k_u z) E_0 \cos(k_\ell z - \omega_\ell t + \psi_0) \end{aligned}$$

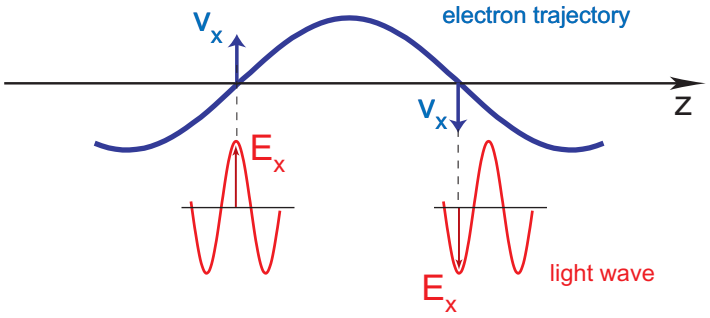

Fig. 12: Condition for energy transfer from electron to light wave.

$$= \quad -\frac{ecKE_0}{2\gamma}\left[\sin((k_\ell + k_u)z - \omega_\ell t + \psi_0) - \sin((k_\ell - k_u)z - \omega_\ell t + \psi_0)\right]$$

We consider the first term. The argument of the sine function is called the *ponderomotive phase*:

$$\psi \equiv (k_\ell + k_u)z - \omega_\ell t + \psi_0 = (k_\ell + k_u)\bar{\beta}ct - \omega_\ell t + \psi_0 \; . \tag{14}$$

There will be a continuous energy transfer from the electron to the light wave if ψ is constant (independent of time) and in the range $0 < \psi < \pi$, the optimum value being $\psi = \psi_0 = \pi/2$. The condition $\psi = const$ can be fulfilled only for a certain wavelength.

$$\psi = const \quad \Leftrightarrow \quad \frac{d\psi}{dt} = (k_\ell + k_u)\bar{v}_z - k_\ell c = 0 \; . \tag{15}$$

Insertion of $\bar{v}_z$ permits to compute the light wavelength:

$$\lambda_\ell = \frac{\lambda_u}{2\gamma^2}\left(1 + \frac{K^2}{2}\right) \; . \tag{16}$$

The condition for resonant energy transfer all along the undulator therefore yields exactly the same light wavelength as is observed in undulator radiation at $\theta = 0$. This is the reason why the spontaneous undulator radiation can serve as a "seed radiation" in the SASE FEL.

Now we look at the second term. Here the phase of the sine function cannot be kept constant since from

$$(k_\ell - k_u)\bar{\beta}ct - \omega_\ell t + \psi_0 = const$$

we would get

$$k_\ell(1 - \bar{\beta}) = -k_u\bar{\beta} \quad \Rightarrow \quad k_\ell = 2\pi/\lambda_\ell < 0$$

which of course is unphysical. Hence the second sine function oscillates rapidly and averages to zero.

3.2 The pendulum equation

We assume "seeding" by an external light source with wavelength λ_ℓ. The **resonant energy** $W_r = \gamma_r\, m_e c^2$ is defined by the equation

$$\lambda_\ell = \frac{\lambda_u}{2\gamma_r^2}\left(1 + \frac{K^2}{2}\right) \; . \tag{17}$$

Let the electron gamma factor be slightly larger, $\gamma > \gamma_r$, and call $\eta = (\gamma - \gamma_r)/\gamma_r$ the relative energy deviation. We assume

$$0 < \eta = \frac{\gamma - \gamma_r}{\gamma_r} \ll 1 \; .$$

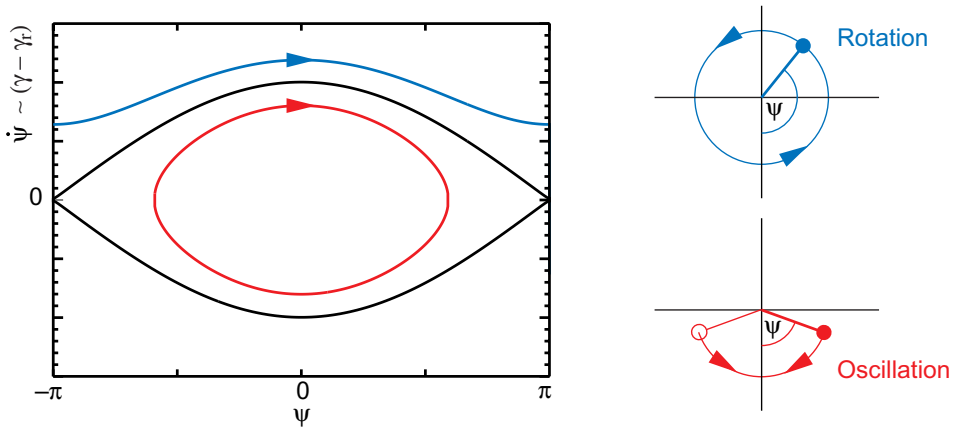

Fig. 13: Phase space curves of a mathematical pendulum.

The energy deviation $\eta\gamma_r\, m_e c^2$ and the ponderomotive phase ψ will both change due to the interaction with the radiation field. The *low-gain FEL* is defined by the condition that the electric field amplitude grows slowly such that $E_0 \approx const$ during one passage of the undulator.

The time derivative of the ponderomotive phase is no longer zero for $\gamma > \gamma_r$:

$$\dot{\psi} = k_u c - k_\ell c \frac{1 + K^2/2}{2\gamma^2} \; .$$

We subtract $0 = k_u c - k_\ell c\,(1 + K^2/2)/(2\gamma_r^2)$, see Eq. (16), and get

$$\frac{d\psi}{dt} = \frac{k_\ell c}{2}\left(1 + \frac{K^2}{2}\right)\left(\frac{1}{\gamma_r^2} - \frac{1}{\gamma^2}\right) \; .$$

From this follows

$$\frac{d\psi}{dt} \approx 2k_u c\eta \equiv \omega' \quad (\omega' \ll k_u c) \; . \tag{18}$$

The time derivative of η is

$$\frac{d\eta}{dt} = -\frac{eE_0 K}{2m_e c\gamma_r^2} \sin\psi \; . \tag{19}$$

Combining Eqs. (18) and (19) we arrive at the so-called *"Pendulum Equation"* of the low-gain FEL

$$\ddot{\psi} + \Omega^2 \sin\psi = 0 \quad \text{with} \quad \Omega^2 = eE_0 K k_u/(m_e\gamma_r^2) \; . \tag{20}$$

3.3 Phase space representation

There is a complete analogy with the motion of a mathematical pendulum (Fig. 13). At small amplitude we get a harmonic oscillation. With increasing angular momentum the motion becomes unharmonic. At very large angular momentum one gets a rotation (unbounded motion). The phase space trajecory for an electron in an FEL can be easily constructed by writing the coupled differential equations (18) and (19) as difference equations and solving these in small time steps. The trajectories for 20 electrons of different initial phases ψ_0 are shown in Fig. 14 for $\gamma = \gamma_r$ and $\gamma > \gamma_r$. In the first case the net energy transfer is zero since there are as many electrons which supply energy to the light wave as there are which remove energy from the wave. For $\gamma > \gamma_r$, however, the phase space picture clearly shows that there is a net energy transfer from the electron beam to the light wave. This will be computed in the next section.

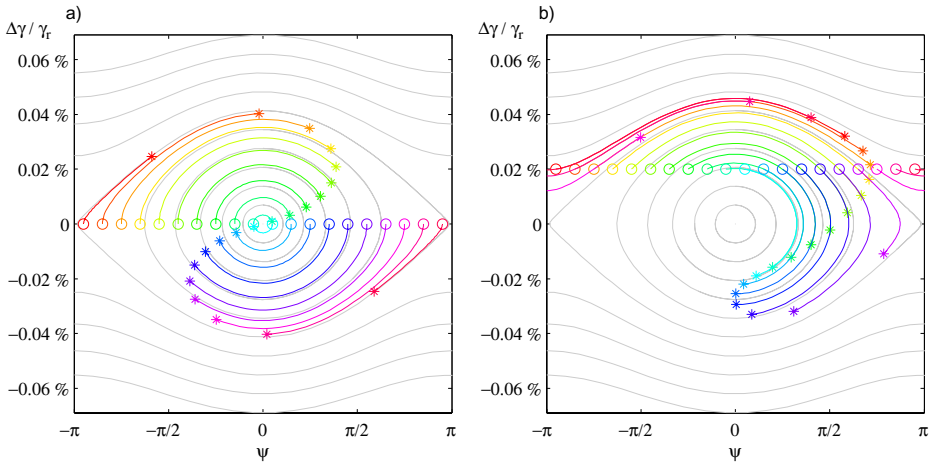

Fig. 14: Phase space trajectories for 20 electrons of different initial phases ψ_0. Left picture: $\gamma = \gamma_r$. The electrons with $\psi_0 < 0$ withdraw energy from the light wave while those with $\psi_0 > 0$ supply energy to the light wave. Obviously the net energy transfer is zero for $\gamma = \gamma_r$. Right picture: $\gamma > \gamma_r$. One can easily see that the net energy transfer is positive.

3.4 Computation of the FEL gain, Madey theorem

The energy (per unit volume) of the light wave is

$$W_{light} = \frac{\varepsilon_0}{2} E_0^2 \ .$$

The energy increase and relative gain caused by one electron are

$$\Delta W_{light} = -m_e c^2 \gamma_r \Delta\eta \qquad G_1 = \frac{\Delta W_{light}}{W_{light}} = -\frac{2 m_e c^2 \gamma_r}{\varepsilon_0 E_0^2} \Delta\eta \ .$$

Here $\Delta\eta$ is the change of the relative energy deviation of the electron upon passing the undulator. We use Eq. (18) to compute this change:

$$\Delta\eta = \frac{\Delta\dot{\psi}}{2 k_u c} \ .$$

Summing over all electrons in the bunch (n_e per unit volume) the total gain becomes

$$G = -\frac{m_e c \gamma_r n_e}{\varepsilon_0 E_0^2 k_u} \cdot < \Delta\dot{\psi} > \ . \tag{21}$$

Here $< \Delta\dot{\psi} >$ denotes the change of the time derivative of the ponderomotive phase, averaged over all electrons. Hence it is this quantity we have to compute.

3.4.1 Phase change in undulator

We multiply the pendulum equation $\ddot{\psi} + \Omega^2 \sin\psi = 0$ with $2\dot{\psi}$ and integrate over time

$$\dot{\psi}^2 - 2\Omega^2 \cos\psi = const \quad \Rightarrow \quad \dot{\psi}(t)^2 = \dot{\psi}_0^2 + 2\Omega^2 [\cos\psi(t) - \cos\psi_0] \ .$$

From Eq. (18)

$$\dot{\psi}_0 = \dot{\psi}(0) = 2c\, k_u\, \eta \equiv \omega'$$

we obtain then

$$\dot{\psi}(t) = \omega' \sqrt{1 + 2(\Omega/\omega')^2 [\cos\psi(t) - \cos\psi_0]} \ . \tag{22}$$

For a weak laser field one finds $(\Omega/\omega')^2 \ll 1$, so we expand the square root up to second order

$$\sqrt{1+x} = 1 + x/2 - x^2/8 \ldots$$

and get

$$\dot{\psi}(t) = \omega' + \frac{\Omega^2}{\omega'} \left[\cos\psi(t) - \cos\psi_0\right] - \frac{\Omega^4}{2\omega'^3} \left[\cos\psi(t) - \cos\psi_0\right]^2 . \tag{23}$$

This equation is solved iteratively.

Zeroth order: $\dot{\psi}_0 = \omega'$, $\Delta\dot{\psi}_0 = 0$.

First order: the phase $\psi(t)$ in first order is obtained by integrating $\dot{\psi}_0$:

$$\psi_1(t) = \psi_0 + \dot{\psi}_0 \cdot t = \psi_0 + \omega' t .$$

We insert this in Eq. (23) to get $\dot{\psi}$ in first order

$$\dot{\psi}_1(t) = \omega' + (\Omega^2/\omega')[\cos(\psi_0 + \omega' t) - \cos\psi_0] . \tag{24}$$

The flight time through the undulator is T, so the change of $\dot{\psi}_1$ when the electron passes the undulator is

$$\Delta\dot{\psi}_1 = (\Omega^2/\omega')[\cos(\psi_0 + \omega' T) - \cos\psi_0] .$$

According to Eq. (21) the gain is obtained by averaging $\Delta\dot{\psi}$ over all particles in the bunch which means that one has to average over all initial phases ψ_0. The result is

$$< \Delta\dot{\psi}_1 >= 0 . \tag{25}$$

The FEL gain is zero in first order. The physical reason is the nearly symmetric initial phase space distribution.

Second order: Equation (24)) is integrated to get ψ in second order:

$$\psi_2(t) = \underbrace{\psi_0 + \omega' \cdot t}_{\psi_1(t)} + \underbrace{(\Omega/\omega')^2[\sin(\psi_0 + \omega' t) - \sin\psi_0 - \omega' t\cos\psi_0]}_{\delta\psi_2(t)} \tag{26}$$

This is inserted in Eq. (23) to compute $\dot{\psi}$ at $t = T$ in second order

$$\begin{aligned} \dot{\psi}_2(T) &= \omega' + (\Omega^2/\omega')[\cos(\psi_0 + \omega' T + \delta\psi_2) - \cos\psi_0] \\ &- \Omega^4/(2\omega'^3)[\cos(\psi_0 + \omega' T + \delta\psi_2) - \cos\psi_0]^2 \end{aligned} \tag{27}$$

$\delta\psi_2 \ll 1 \quad \Rightarrow \quad \cos(\psi_0 + \omega' T + \delta\psi_2) \approx \cos(\psi_0 + \omega' T) - \delta\psi_2 \sin(\psi_0 + \omega' T)$

$$\begin{aligned} \cos(\psi_0 + \omega' T + \delta\psi_2) &\approx \cos(\psi_0 + \omega' T) \\ &- (\Omega/\omega')^2 \sin(\psi_0 + \omega' T)[\sin(\psi_0 + \omega' T) - \sin\psi_0 - \omega' T\cos\psi_0] \end{aligned}$$

Averaging over all start phases ψ_0 yields
$< \cos(\psi_0 + \omega' T + \delta\psi_2) >= (1/2)(1 - \cos(\omega' T) - \omega' T \sin(\omega' T))$.
From this we get

$$< \Delta\dot{\psi}_2 >= -(\Omega^4/\omega'^3)[1 - \cos(\omega' T) - (\omega' T/2)\sin(\omega' T)] .$$

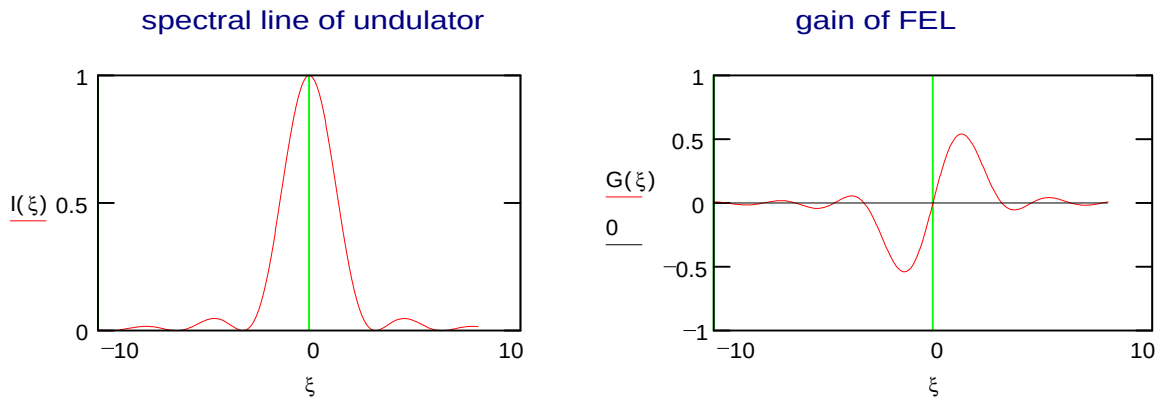

Fig. 15: The normalized lineshape curve of undulator radiation and the gain curve (arbitrary units) of the low-gain FEL as a function of $\xi = \pi N_u \, (\omega - \omega_\ell)/\omega_\ell$.

Remembering that $T = N_u \lambda_u / c$ is the flight time through the undulator and $\xi = \omega' T/2$ one obtains

$$\begin{aligned} < \Delta\dot{\psi}_2 > &= -\frac{\Omega^4}{\omega'^3}[1 - \cos(2\xi) - \xi \, \sin(2\xi)] \\ &= \frac{N_u^3 \lambda_u^3 \Omega^4}{8c^3} \cdot \frac{d}{d\xi} \left(\frac{\sin \xi}{\xi} \right)^2 \end{aligned}$$

The FEL gain function (21) is hence

$$G(\xi) = -\frac{\pi \, e^2 K^2 N_u^3 \lambda_u^2 \, n_e}{4\varepsilon_0 m_e c^2 \gamma_r^3} \cdot \frac{d}{d\xi} \left(\frac{\sin^2 \xi}{\xi^2} \right) \tag{28}$$

We have proven the *Madey Theorem* which states that the FEL gain curve is given by the negative derivative of the line-shape curve of undulator radiation. This is shown in Fig. 15.

4 High-gain FEL

4.1 General principle

The essential feature of the high-gain FEL is that a large number of electrons radiate coherently. In that case, the intensity of the radiation field grows quadratically with the number of particles: $I_N = N^2 \, I_1$. If it were possible to concentrate all electrons of a bunch into a region which is far smaller than wavelength of the radiation then these N particles would radiate like a "point macroparticle" with charge $Q = -Ne$, see Fig. 16. The big problem is, however, that this concentration of some 10^9 electrons into a tiny volume is totally unfeasible, rather even the shortest particle bunches are much longer than the FEL wavelength. The way out of this dilemma is given by the process of **micro-bunching** which is based on the following principle: those electrons which lose energy to the light wave travel on a cosine trajectory of larger amplitude than the electrons which gain energy from the light wave The result is a modulation of the longitudinal velocity which eventually leads to a concentration of the electrons in slices which are shorter than λ_ℓ . The result of a numerical simulation of this process is shown in Fig. 17. The particles within a micro-bunch radiate coherently. The resulting strong radiation field enhances the micro-bunching even further. The result is a "collective instability", leading to an exponential growth of the radiation power. The ultimate power is $P \propto N_c^2$ where N_c is the number of particles in a coherence region. A typical value is

$$N_c \approx 10^6 \quad \Rightarrow \quad P_{\rm FEL} = 10^6 P_{undulator} \, .$$

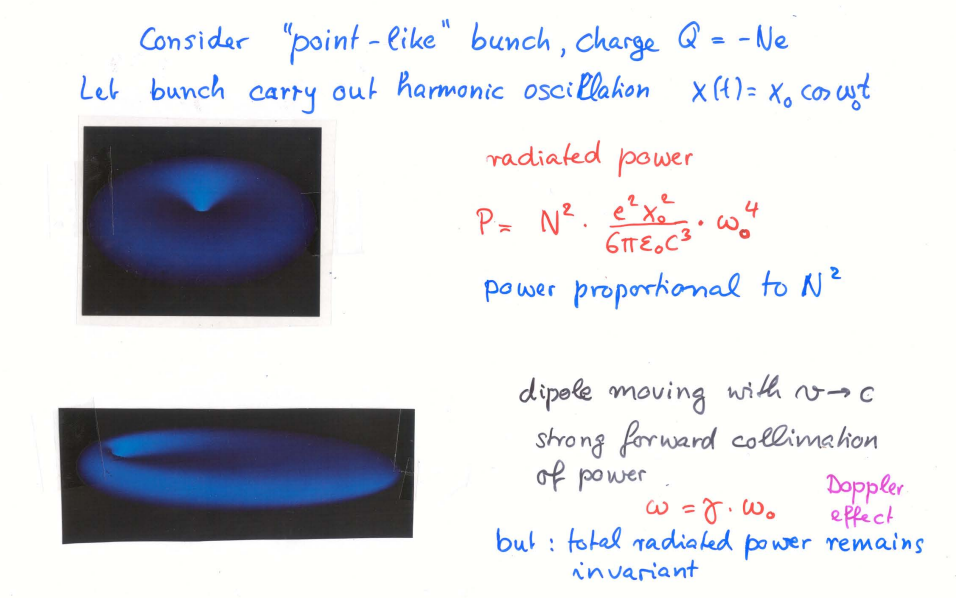

Fig. 16: Radiation from a point-like macroparticle

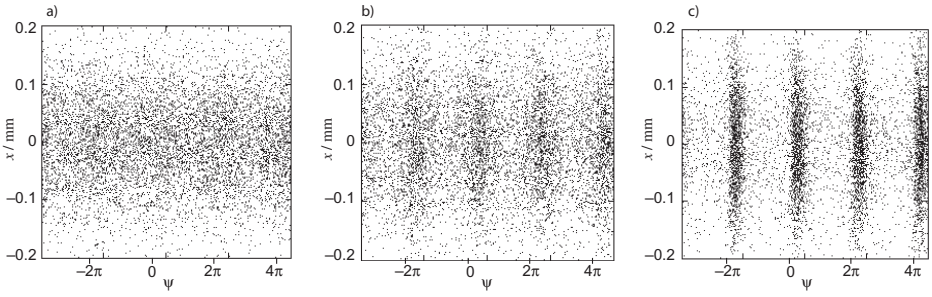

Fig. 17: Numerical simulation of microbunching. (Courtesy S. Reiche).

4.2 Approximate analytical treatment and experimental results

An approximate analytic description of the high-gain FEL requires the self-consistent solution of the coupled pendulum equations and the inhomogeneous wave equation for the electromagnetic field of the light wave. In the one-dimensional FEL theory the dependencies on the transverse coordinates x, y are disregarded. The wave equation for the radiation field E_x reads

$$\frac{\partial^2 E_x}{\partial z^2} - \frac{1}{c^2}\frac{\partial^2 E_x}{\partial t^2} = \mu_0 \frac{\partial j_x}{\partial t}$$

where the current density $\vec{j}$ is generated by the electron bunch moving on its cosine-like trajectory. In addition, one has to consider the longitudinal *space charge field* E_z which is generated by the gradually evolving periodic charge density modulation. After a lot of tedious mathematical steps and several simplifying assumptions one arrives at a third-order differential equation for the amplitude of the electric field of the light wave:

$$\frac{d^3\tilde{E}_x}{dz^3} - 4ik_u\eta\frac{d^2\tilde{E}_x}{dz^2} + (k_p^2 - 4k_u^2\eta^2)\frac{d\tilde{E}_x}{dz} - i\Gamma^3\tilde{E}_x(z) = 0\,. \tag{29}$$

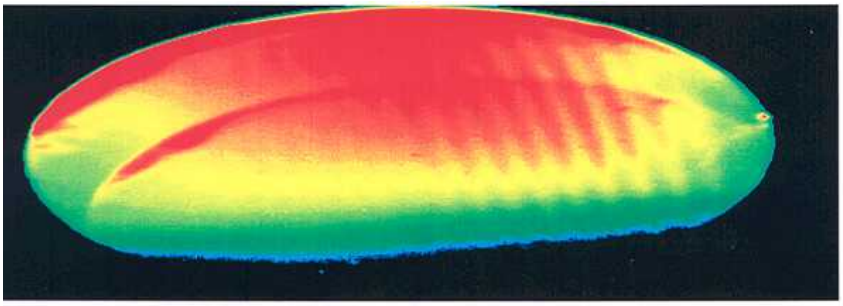

Fig. 18: Observation of microbunching at the 60 μm FEL Firefly.

Here we have introduced the *gain parameter* Γ and a parameter k_p

$$\Gamma = \left(\frac{\mu_0 K^2 e^2 k_u n_e}{4\gamma^3 m_e} \right)^{\frac{1}{3}} \quad , \quad k_p = \sqrt{\frac{4\gamma^2 c \Gamma^3}{\omega K^2}} \tag{30}$$

and assumed that the electron beam has negligible energy spread.

This third-order differential equation can be solved analytically. For the case $\gamma = \gamma_r$ one obtains

$$\tilde{E}_x(z) = A_1 \exp\left(-i\Gamma z\right) + A_2 \exp\left(\frac{i+\sqrt{3}}{2} \Gamma z \right) + A_3 \exp\left(\frac{i-\sqrt{3}}{2} \Gamma z \right) \ . \tag{31}$$

The second term exhibits exponential growth as a function of the position z in the undulator. The electric field grows exponentially as $\exp(\frac{\sqrt{3}}{2}\Gamma z)$, the power grows as $\exp(\sqrt{3}\Gamma z)$. The gain parameter Γ is related to two parameters which are in widespread use: the Pierce parameter and the power gain length

$$\rho_{pierce} = \frac{\lambda_u \Gamma}{4\pi} \qquad L_g = \frac{1}{\sqrt{3}\,\Gamma} \ . \tag{32}$$

The above calculations, which have been sketched only very briefly, indicate that there is an onset of an "instability", leading to a progressing microbunching and an exponential increase in radiation power along the undulator. A quantitative treatment requires elaborate numerical simulations (see Fig. 17). Microbunching has been experimentally observed at the 60 μm FEL Firefly at Stanford University, see Fig. 18. The exponential growth of radiation power and the progressing microbunching in a long undulator are depicted in Fig. 19. One characteristic but quite undesirable feature of a SASE FEL is the presence of fluctuations which are due to the stochastic nature of the initiating undulator radiation. The light pulse energy fluctuates from pulse to pulse, and the same applies for the wavelength and the time structure. As an example I show in Fig. 20 the measured wavelength distribution of several FEL pulses together with the average over 100 pulses. The origin of the large fluctuations is that small statistical fluctuations in the incoming undulator radiation are strongly amplified in the exponential growth region (see Fig. 19). There are so-called "seeding schemes" under development where radiation of the desired wavelength is produced in a short undulator, passed through a monochromator and then used as seed radiation for the FEL process. Here one can expect much higher monochromaticity of the final FEL radiation. In spite of the fluctuations the SASE radiation is highly coherent as demonstrated by the double-slit interference patterns in Fig. 21.

Bibliography

K.Wille, The Physics of Particle Accelerators, Oxford University Press 2001

E. L. Saldin, E. A. Schneidmiller, M. V. Yurkov, The Physics of Free Electron Lasers, Springer 2000

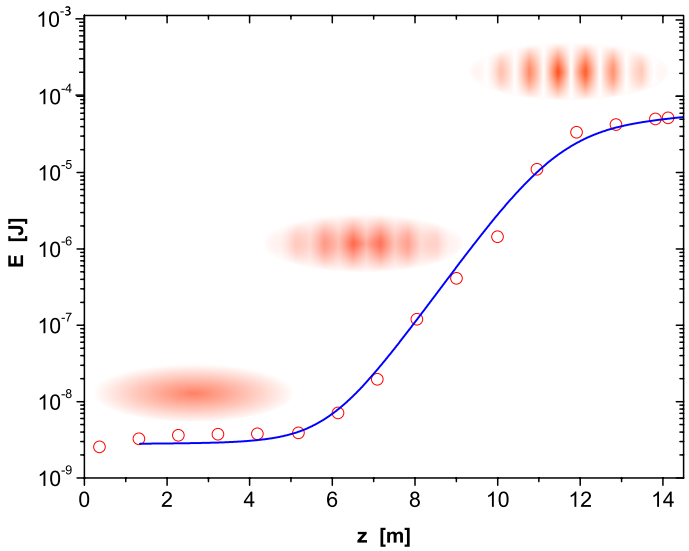

Fig. 19: The exponential growth of radiation power as a function of undulator length. The data at $\lambda = 100$ nm have been obtained at the SASE FEL of the TESLA Test Facility at DESY. The progressing microbunching is indicated schematically.

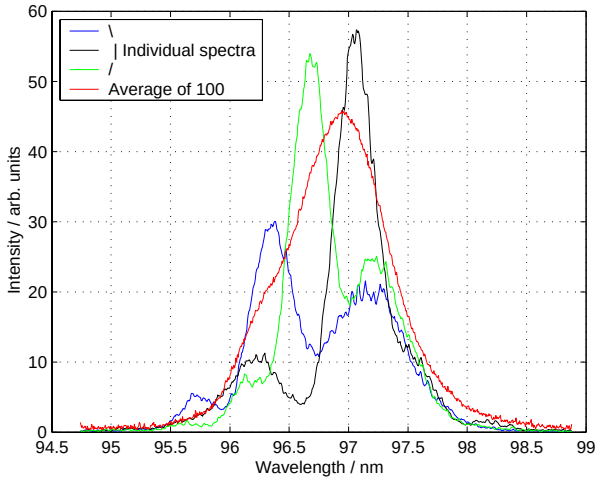

Fig. 20: The measured spectra of three pulses in the SASE FEL at DESY. Also shown is the average spectrum of 100 pulses.

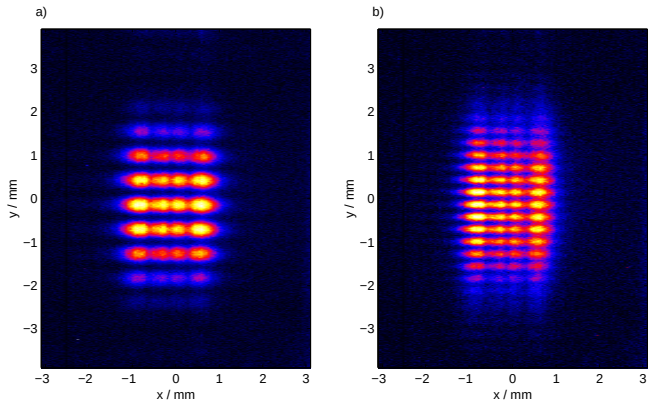

Fig. 21: Measured double-slit diffraction patterns at 100 nm FEL wavelength. The separation of the horizontal slits is 0.5 resp. 1 mm.